ACS APPLIED MATERIALS & INTERFACES

Research Article

www.acsami.org

Fractal Dimension of Sparkles in Automotive Metallic Coatings by Multispectral Imaging Measurements

José M. Medina,* José A. Díaz, and Carlos Vignolo†

Facultad de Ciencias, Departmento de Óptica, Edificio Mecenas, Universidad de Granada, 18071 Granada, Spain

Supporting Information

ABSTRACT: Sparkle in surface coatings is a property of mirror-like pigment particles that consists of remarkable bright spots over a darker surround under unidirectional illumination. We developed a novel nondestructive method to characterize sparkles based on the multispectral imaging technique, and we focused on automotive metallic coatings containing aluminum flake pigments. Multispectral imaging was done in the visible spectrum at different illumination angles around the test sample. Reflectance spectra at different spatial positions were mapped to color coordinates and visualized in different color spaces. Spectral analysis shows that sparkles exhibit higher reflectance spectra and narrower bandwidths. Colorimetric analysis indicates that sparkles present higher lightness values and are far apart from the bulk of color coordinates spanned by the surround. A box-counting procedure was applied to examine the fractal organization of color coordinates in the CIE 1976 $L^*a^*b^*$ color space. A characteristic noninteger exponent was found at each illumination position. The exponent was independent of the illuminant spectra. Together, these results demonstrate that sparkles are extreme deviations relative to the surround and that their spectral properties can be described as fractal patterns within the color space. Multispectral reflectance imaging provides a powerful, noninvasive method for spectral identification and classification of sparkles from metal flake pigments on the micron scale.

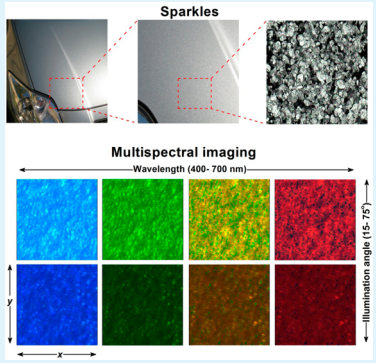

KEYWORDS: *sparkles, flake-shaped pigments, metallic coatings, multispectral imaging, texture engineering, box-counting analysis*

INTRODUCTION

Sparkles in surface materials are tiny bright spots of reflected light from plate-shaped particles often observed over a darker surround under unidirectional illumination (e.g., direct sunlight).[1−5] In manufactured goods, sparkles are usually found in toothpastes, cosmetics, pearlescent and metallic coatings, and others;[1−4,6] they sparkle like many materials in nature, such those arising from diamonds, gems, snowflakes, sands, and so forth.[5] Protective metallic coatings are widely used in industry, and they enhance the visual impression of objects by mimicking the appearance of metals. Metallic finishes incorporate metal flake pigments parallel to the substrate in a transparent medium. Metal flakes act as mirror-like reflectors on the micron scale and are responsible for lightness changes as a function of the viewing angle.[6−8] Sparkles are created by those individual flakes that are non-parallel-oriented in the surrounding medium[1,2,6] (also called sparkling, microbrightness, glint impressions, diamonds, and optical roughness).[1,3,4,6] Sparkles depend on the illumination and viewing angle positions as well as the morphology of flake pigments and their size, density, rheology additives, paint application method, and so forth.[3,4,6] Sparkles are of great interest as a design tool because they lend a strong impact by creating subdued and crystal-like textures and because they enhance the overall color impression in cosmetics, plastics, household electrical products, packaging, printed materials, and others.[1,2,6,8] Visual test methods[3,4,9] have been used for subjective visual judgments of texture appearances in metallic coatings. Digital image analyses[3,6,9−12] have also been used for statistical counts of sparkle effects from reflecting particles. Relatively little attention has been focused on the spectral and colorimetric properties of sparkles.[1−4,6,7,9,13,14] Standard multiangle spectrophotometers cannot be used to measure sparkles in metallic coatings; they are limited by their spatial resolution because they often average over spot diameters of very few millimeters and because optical measurements of individual flake pigments are diluted.[1,6,13] Research on the micro appearance of metallic coatings is crucial for an accurate description of sparkle effects, which traditional spectroscopy methods and visual methods using the naked eye alone cannot judge, as well as other texture aspects (e.g., graininess).[1,6]

Multispectral imaging is a nondestructive technique that combines both spectroscopic and digital image analysis with high spatial resolution. Such imaging has found diverse applications.[15,16] Multispectral data are generated as a 3D data cube or image cube,[15] with two spatial dimensions, i.e., the x and y axes (the size of the digital image), and a third, the spectral axis, sampled over a discrete number of wavelength intervals.[15,16] Multispectral systems can generate thousands of reflectances, one at each pixel position in the field of view, providing more

Received: April 2, 2014
Accepted: June 19, 2014
Published: June 19, 2014

spectral and spatial information than the naked eye or red, green, and blue (RGB) camera-based systems.[14,17] This affords us an important advantage for the detection and selection of sparkles with distinct spectral signatures because the entire reflectance spectra is available at each pixel in the imaged scene.

In the present work, we investigated the spectral and colorimetric properties of sparkles in metallic coatings using multispectral imaging on the micron scale, and we focused on conventional metallic coatings in automotive finishes containing aluminum flake pigments. Automotive coatings are probably one of the most important coating sectors, which include the latest developments in flake-shaped pigments (also called effect pigments).[6−8] Although researchers have developed various multispectral systems for the analysis of metallic coatings,[14,17] they have not investigated the spectral and colorimetric analysis of sparkles. The importance of effect pigments in modern metallic coatings and the complexity of the different industrial paint application processes demand innovative methods to measure the dependency between sparkles and their surround on the microscopic scale. Here, we present a novel method to characterize sparkles based on their colorimetric properties. We have examined the reflectance spectra of sparkles in the visible spectrum at different illumination angle positions, from near to far from surface normal. Reflectance spectra at different pixels are transformed to color coordinates in an appropriate 3D perceptual color space that gives a representation of human color vision.[6,14,18,19] Therefore, reflectance spectra at different pixel positions are specified by only three numbers, or the color coordinates,[18] and the spatial microstructure of paint coatings is mapped into characteristic color maps.[6,14,18] We suggest that these color maps contain key information to understand the spectral properties of sparkles relative to their surround. We assume that color coordinates at each pixel in the multispectral sensor represent a spatial position in the paint film with a specific spatial resolution. Some pixels have color coordinates that are close to the color coordinates of nearby pixels. There are also pixels that register tiny brighter spots in the paint film, attributed in part to sparkles, where their color coordinates lie quite distant from the main aggregate of the colorimetric data. All of these color coordinates are related to each other because they are derived from the same paint application process and should be analyzed together. The fundamental approach is to measure how the color coordinates at different pixel positions cover the entire color space. Color maps occupied by metallic coatings do not usually show a well-defined Euclidean form, but they are strongly inhomogeneous, exhibiting irregular shapes, cluster agglomerations, and tree-like patterns in the color space.[14] We assume that each color map can be treated as a structure in which color coordinates are grouped in the same way at different scales, i.e., a self-similar structure. It has been shown that this approach provides a valuable framework to analyze the fractal colorimetric organization of everyday scenes[20,21] and artistic paints.[19,22,23] In the present study, we propose a similar approach in the research of the colorimetric properties of sparkles in surface coatings. We have applied a box-counting procedure[19,21,22] to examine the fractal colorimetric organization spanned by the metallic coatings at different illumination angles. We propose the use of box-counting because it is one of the most commonly used methods to describe the fractal dimension of many practical fractals (e.g., the lengths of coasts and land frontiers, fracture surfaces, agglomeration of aerosols and colloids, etc.).[19,21−25] Furthermore, there are fast computer algorithms for implementing box-counting using large data sets embedded in 2D as well as in other dimensional spaces. In box-counting, all of the boxes, $N(r)$, that intersect with color coordinates are counted as a function of their box size, r. For instance, the box size, r, is reduced iteratively, and the total number of occupied boxes that cover the entire pattern is counted. If scaling similarity prevails, then the pattern behaves as a fractal, and the counts should follow a power law, $N(r) \cong r^{-D_B}$. The parameter D_B is the scaling factor, a unique fractional number less than the dimension of the embedded Euclidean space that identifies the space-filling property of the pattern, i.e., the box-counting dimension or how rugged or irregular a complex structure is.[19,21,24,25] For a large set of fractal objects, the box-counting dimension, D_B, is closely related to their fractal dimension as measured by the Hausdorff dimension, which is often more difficult to compute.[19,21,22,24,25]

EXPERIMENTAL SECTION

Material Synthesis. Two different metallic samples from car coatings were prepared and analyzed. Both metallic coatings are representative of automotive original equipment manufacturer (OEM) paints.[8] They are solvent-borne two-layer systems sprayed on steel anchor panels. They consist of a basecoat, where pigments are dispersed in a transparent medium or binder, and a clearcoat, with a transparent lacquer that provides a high-quality gloss and protection.[8] The lacquer and the binder were the same in both metallic samples. The metallic coatings are complex dispersive media that follow the standards in automotive OEM coatings.[8] The first metallic coating (metallic blue 1) contains lenticular or silver dollar[6−8] aluminum flake pigments. Silver dollar aluminum flakes have rounded edges and are very flat. They reflect light by specular reflection and provide lower scattering at the borders as well as lighter and more brilliant effects than other types of aluminum pigments.[6−8] The particle size distribution of the silver dollar aluminum pigment used has a narrow range and has a median particle diameter of 16 μm. Aluminum flakes were mixed with organic indanthrone particles with color index, Pigment Blue 60, and average particle size less than 1 μm. Blue indanthrone particles are light-absorption pigments that provide a deep transparent blue and a weak red and are often used in high-performance OEM metallic finishes.[6−8] The mixture of pigment−aluminum in the color recipe was 50/50 wt %. The metallic blue paint was uniformly spread on the anchor panel using the standard pneumatic atomization method.[8] The evaporation of solvents was performed in an oven following a standard procedure used in OEM coatings.[8] Solvent evaporation shrinks the coating thickness and is an important mechanism in metallic finishes to assemble the aluminum flakes parallel to the substrate.[8,12,26] Sparkles were visually noticeable in a clear sky under direct sunlight as well as in a conventional light booth using a panel rack.[4,6] The second metallic coating (metallic blue 2) was created for test comparisons with metallic blue 1, and it was intended to simulate a failure analysis in OEM coatings. Metallic blue 2 has the same pigment composition and formulation and the paint was uniformly spread on a panel in the same way as in metallic blue 1. However, film shrinkage was modified by leaving the panel for more time than prescribed in OEM coatings.[8] Modification of coating film thickness by excessive solvent evaporation produces physical damage that leads to color mismatch, gloss variation, irreversible perturbations in the orientation of aluminum flakes, and other forms of damage.[6,8,27]

Structural Characterization. Structural analysis of metallic coatings was undertaken by means of optical and scanning electron microscopy (SEM). Optical images of metallic panels were captured with a conventional digital color camera (Canon PowerShot SD1000). Reflection color photomicrographs were obtained by using an optical microscope (Nikon Optiphot-100) connected to a charge-couple device (CCD) color video camera (Sony DXC-107AP). A SEM micrograph of a small bluish region of each metallic panel was obtained by removing the lacquer. Each sample was coated with a thin film of gold palladium alloy (80/20 wt %) using a 208HR Cressington sputter coater coupled

to a MTM-20 Cressington thickness controller and examined using a NOVA 200 nano SEM FEI instrument.

Multispectral Imaging Setup. The multispectral acquisition system has been reported previously,[28] but it has been adapted to the study of sparkles in automotive metallic coatings in this work. Figure 1

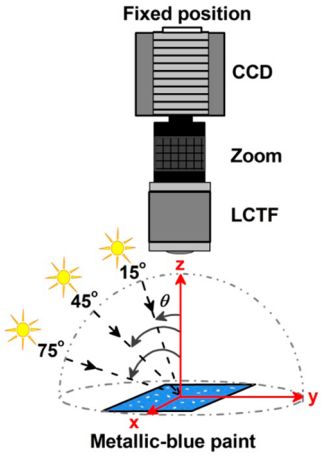

Figure 1. Schematic illustration of the multispectral imaging system.

shows a schematic representation of the multispectral system. The device consisted of a liquid crystal tunable filter (LCTF) (Varispec VS-VIS2-10HC-35-SQ) placed in front of a conventional objective zoom lens (Navitar Zoom 7000 18:108 mm) attached to a 12 bit monochrome CCD (Retiga QImaging SVR1394). The LCTF, zoom lens, and CCD sensor array were in a fixed position, and they were aligned exactly perpendicular to the sample.

The illumination system uses a 150 W compact and highly stable mercury−xenon (Hg−Xe) lamp (Hamamatsu L9588-04). Light from the Hg−Xe lamp is collected by a 1.5 m light guide fiber (Hamamatsu A10014-50-010). The end of this light guide has a condenser lens (Hamamatsu E5147-06) with a focal length of 50 mm designed to provide a squared uniform light distribution (40 × 40 mm) on the side perpendicular to the surface sample. The light guide was mounted in a 360° continuous rotation stage (Thorlabs RBB12). A neutral density filter with 24.94% transmittance (Oriel 59341/B) was mounted in front of the condenser lens to decrease the amount of light reaching the test sample. Multispectral imaging was performed at three different illumination angle positions, θ, to capture the color dynamics of sparkles from near to far from the surface normal: 15, 45, and 75° (Figure 1). This multiangle illumination configuration is very similar to that used in digital image analyses of sparkles using a monochrome CCD camera such as in the BYK-mac instrument.[3,6,9] The illumination angle of 45° simulates the standard measurement geometry for diffuse reflectance CIE 45°/0° (Commission Internationale de l'Éclairage).[6,18]

Experimental Procedure and Calibration. Multispectral measurements were controlled using custom software in a dark room.[28] Measurements were started after the Hg−Xe lamp had been lit for more than 5 min to ensure light output stability. The CCD camera and the LCTF have been fully tested in previous studies in our laboratory.[28] The LCTF was tuned from 400 to 700 nm in steps of 10 nm, giving a total of 31 different spectral bands. The exposure time at each wavelength was calculated automatically by ensuring that the number of digital counts did not exceed 85% of the maximum permitted at any pixel in the multispectral image. Chromatic aberration was controlled by focusing the zoom lens manually. The spectral reflectance factor is based on a white reflectance standard,[18] and it was calculated at each pixel of the imaged surface using the two-point correction method. This method is standard in spectral imaging and is described elsewhere[14−16] (see the Supporting Information). The white flat-field correction is the reference white standard that determines the reflectance factor at each pixel for each of the 31 different spectral bands.[15,16] It was obtained by defocusing a 99% white diffuse reflectance Spectralon standard[29] to avoid spatial noise from the inhomogenous structure

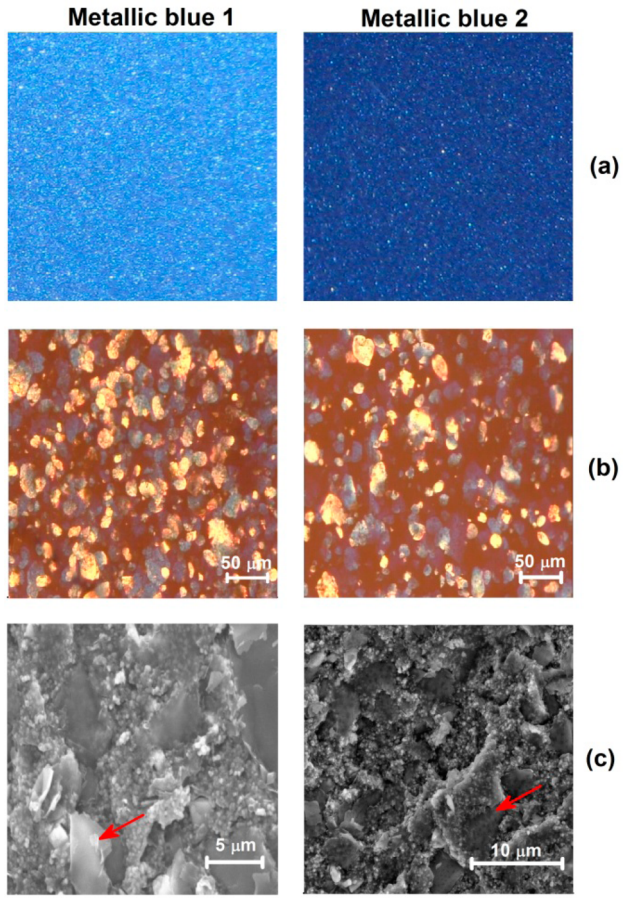

Figure 2. Structural analysis of two representative solvent-borne clearcoat−basecoat automotive metallic coatings labeled as metallic blue 1 and metallic blue 2. (a) Example of sparkles in metallic coatings. Optical images in a clear sky under direct sunlight. (b) Optical micrographs (bright-field illumination) show the presence of silver dollar aluminum flakes covered by blue indanthrone pigment particles. (c) Scanning electron micrographs after the lacquer was removed. Red arrows indicate an example of aluminum flakes without (left panel) and with (right panel) physical damage produced by excessive evaporation of the solvent.

under high magnification.[14,16] The Spectralon was illuminated by the Hg−Xe lamp at 15, 45, and 75° (Figure 1). The dark-field correction is the reference black that determines the level of dark noise.[15,16] It was obtained under the same conditions as those of the white flat field but without the sample holder and with the light source off, preventing any residual light from entering the CCD camera. To minimize spatial nonuniform effects from the CCD sensor and LCTF,[28] a user-defined region of interest (ROI) consisting of a square of 201 × 201 pixels was selected at the center of the captured image cube. The multispectral imaging system had a spatial resolution of 14.4 μm/pixel under the operating conditions.

Spectral calibration of the multispectral system was performed using a common procedure in color imaging.[14,16,17] We have compared the shape of the mean spectral reflectance factor averaged over 201 × 201 = 40 401 reflectances of Macbeth color patches[28,30] with those provided by standard spectrophotometry.[14,16,17] For each metallic sample, we further tested the mean spectral reflectance factor obtained using the multispectral system with those measurements obtained by means of a commercial spectrophotometer (see the Supporting Information).

Colorimetric Performance. The colorimetric methods used in the present study are standard and are discussed elsewhere.[6,18] Reflectance spectra at different pixel positions were transformed to the CIE XYZ tristimulus values by using the CIE 1931 2° color matching

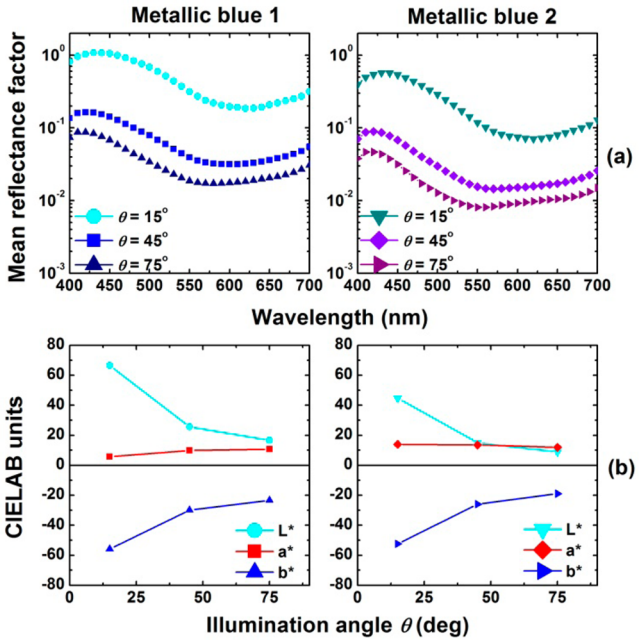

Figure 3. Spectral and colorimetric average values of metallic coatings. (a) Semilogarithmic plot of the mean spectral reflectance factor as a function of the illumination angle, θ, as measured by multispectral imaging. (b) CIELAB values as a function of the illumination angle. Data were calculated using the CIE 2° standard observer and the CIE standard illuminant D65.

functions at discrete wavelength intervals.[6,18] Next, the XYZ tristimulus values at each pixel position were converted into the sRGB color space. The sRGB color space is intended for color representation in displays. In box-counting analysis, the XYZ tristimulus values were converted into the CIE 1976 $L^*a^*b^*$ perceptual color space (CIELAB). The CIELAB color space is device-independent; it correlates with human color vision and is recommended for color representation of pigmented coatings. The color plane is defined by the a^* and b^* orthogonal axes. The coordinate a^* correlates with red ($a^* > 0$) and green ($a^* < 0$), and the b^* coordinate with yellow ($b^* > 0$) and blue ($b^* < 0$). The L^* axis is a measure of lightness that correlates with black ($L^* = 0$) and perfect white ($L^* = 100$). The L^* axis is orthogonal to the (a^*,b^*) color plane.[6,18] Four different illuminants were used: D65, A, FL2, and FL11. The CIE standard illuminant D65 simulates daylight conditions. All of the illuminant spectra are typical in industrial color testing.[6,18]

■ ANALYSIS

Data Analysis. A preprocessing study was performed on reflectance spectra before applying box-counting analysis to color coordinates by using principal components analysis (PCA). PCA is a robust statistical method that has been used for many applications on multivariate data.[16,31−33] Here, we have applied PCA for noise reduction from the multispectral system. Noise reduction is important because it could contaminate the colorimetric analysis of sparkles by box-counting. We have used a method based on the estimation of the eigenvalues from PCA and their uncertainty.[16,31−33] Original reflectance spectra were projected into a low-dimensional space that explains most of the total variance and therefore the noise arising from the multispectral system can be filtered. (see the Supporting Information).

We restricted the box-counting analysis to 2D L^*b^* planes in the CIELAB color space. This issue will be explained later. In 2D, boxes become flat and are represented by grids. Binary images (black pixels over white background) were produced with the same resolution (300 dots/inch) at illumination angles, θ, of 15, 45, and 75°, separately. Then, box-counting was performed using *FracLac*, a plugin for *ImageJ*.[34,35] For each image, grid localization was changed randomly to perform 12 different box-counting configurations. In each configuration, the grid size, r, increases linearly between a maximum and a minimum. The increment was fixed and was calculated automatically. The maximum grid size represented 45% of the image size. The minimum grid size was lower than or equal to 201 × 201 = 40 401 pixels, i.e., the total number of pixels of the user-defined ROIs. Linear regression analysis of the total number of grids, $N(r)$, as a function of the grid size, r, was performed in a double-logarithmic plot. The goodness-of-fit was evaluated using the R^2 coefficient. The resulting box-counting dimension, D_B, was averaged over the 12 different box-counting configurations. Therefore, for each metallic coating, three different values of D_B were obtained, one at each illumination angle, θ. Box-counting analysis of color coordinates at different illumination spectra were represented in a 3D space where each axis indicates the box-counting dimension, D_B, at illumination angles, θ, of 15, 45, and 75°, respectively.

■ RESULTS AND DISCUSSION

Structural Analysis. Figure 2 summarizes the structural analysis of metallic coatings. Optical images under direct sunlight in Figure 2a indicate a color mismatch and texture differences between both samples. Optical micrographs in Figure 2b and SEM micrographs in Figure 2c confirm that metallic blue 2 has more subdued sparkle effects resulting from aluminum flakes.

Multispectral Analysis. Figure 3a shows the mean spectral reflectance factor at illumination angles, θ, of 15, 45, and 75° for each metallic coating. Each mean reflectance was obtained from the average over 40 401 reflectances. Mean reflectance curves are similar at different illumination angles. Aluminum flakes mainly scale the reflectance factor in the vertical axis. The wavelength at which the reflectance factors are maxima is not strongly dependent upon the illumination angle, θ. The spectral reflectance factor of metallic blue 1 was higher at all illumination angles. Figure 3b shows the corresponding CIELAB values as a function of the illumination angle.

Metallic blue 1 shows higher lightness ($L^* > 0$) and blue values ($b^* < 0$). Lightness changes are produced by aluminum flakes.[6−8] Because metallic blue 2 has the same pigment composition and formulation as metallic blue 1, Figure 3b suggests that fewer aluminum flakes contribute to its own metallic appearance or that the aluminum flakes become orientated differently due to larger solvent evaporation (cf. Figure 2). Blue changes are due to aluminum flakes covered by blue indanthrone particles. Red values ($a^* > 0$) remain nearly constant and are exclusively attributed to a weak reddish effect from indanthrone pigment particles.[6,7]

Figure 4a shows the entire ROIs of the metallic blue 1 and metallic blue 2 samples at illumination angles, θ, of 15, 45, and 75° in the sRGB color space. This gives a total of six different spatial color maps placed in a matrix arrangement of two rows by three columns. Each spatial color map shows the micro appearance of each metallic coating using the multispectral system and consists of 201 × 201 pixels that cover an area of 8.4 mm^2 each. Metallic blue 1 confirms texture effects at the surface that are different from those of metallic blue 2 (cf. Figure 2). Sparkle effects are predominant at 15° and more noticeable in metallic blue 1. Open squares (207.4 μm^2 each)

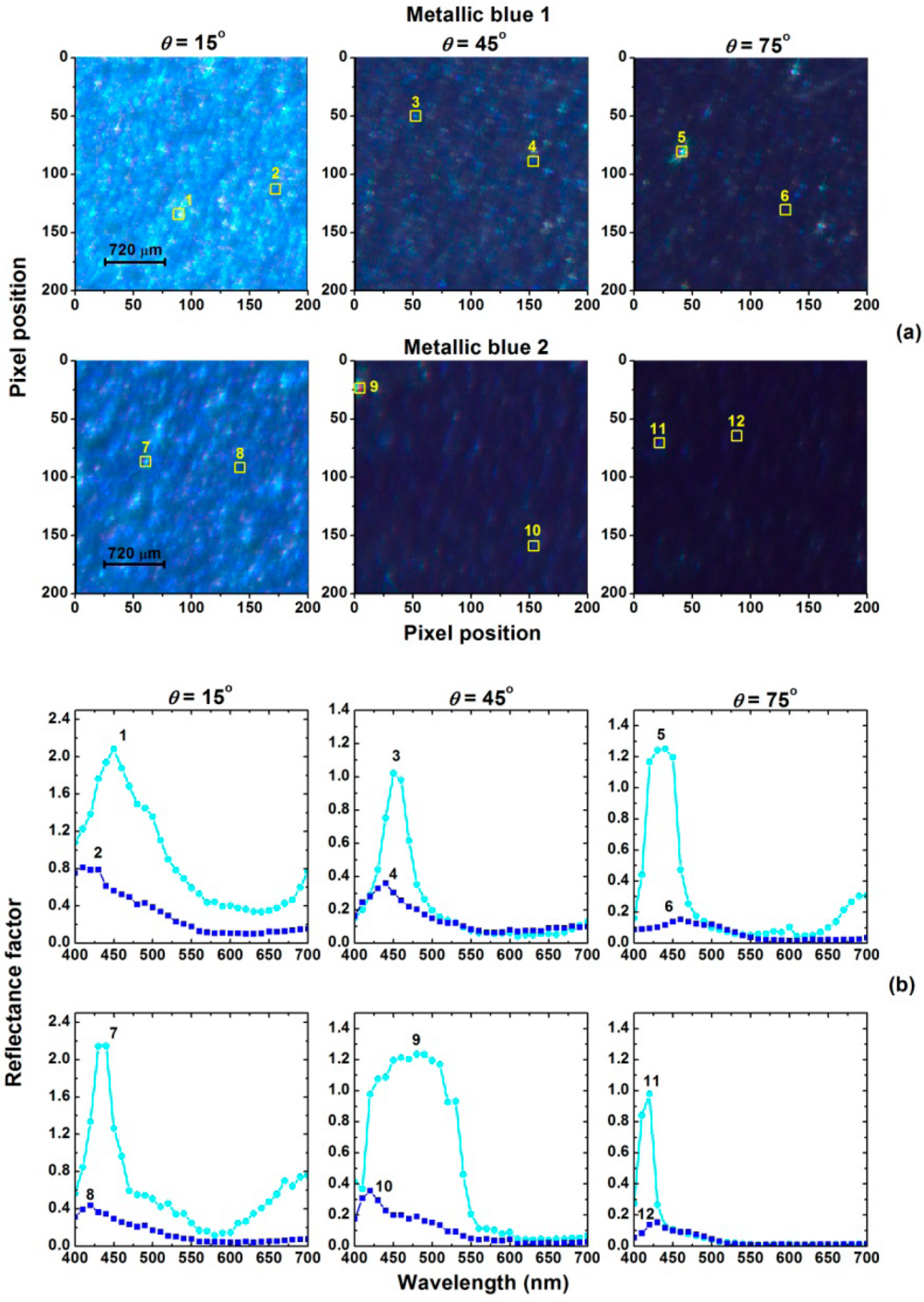

Figure 4. (a) Entire imaged areas (201 × 201 pixels) measured with the multispectral system. At each CCD pixel's position, reflectance spectra were transformed to CIE XYZ tristimulus values and then converted to the sRGB color space. Open squares labeled 1, 3, 5, 7, 9, and 11 indicate six representative CCD pixels of sparkles at different spatial positions and illumination angles in metallic blue 1 and metallic blue 2, respectively. Open squares labeled 2, 4, 6, 8, 10, and 12 show six representative CCD pixels of the surround at different spatial locations and illumination angles in metallic blue 1 and metallic blue 2, respectively. (b) Spectral reflectance factor of selected CCD pixels at different illumination angles from panel a.

mark six representative groups of CCD pixels at different spatial locations and illumination angles. The spectral reflectance factors of these groups of pixels are plotted in Figure 4b. In all of the examples, the spectral reflectance factor of sparkles is higher than the surround, especially in the bluish part of the visible spectrum. The reflectance factor often exceeds unity due to the presence of aluminum flakes (cases 1, 3, 5, 7, and 9). This is possible because the reflectance factor is defined as a function of a white reflectance standard.[6,18,29] Reflectance factors higher than unity are totally compatible with the principle of conservation of energy,[6,18] and they are usual in surface coatings containing effect pigments.[6] In some examples, the reddish part of the reflectance factor corresponds only to the presence of indanthrone pigment particles (cases 1, 5, and 7). The full width at half-maximum of sparkles was narrower than the surround except in metallic blue 2 at $\theta = 45°$ (cases 9 and 10).

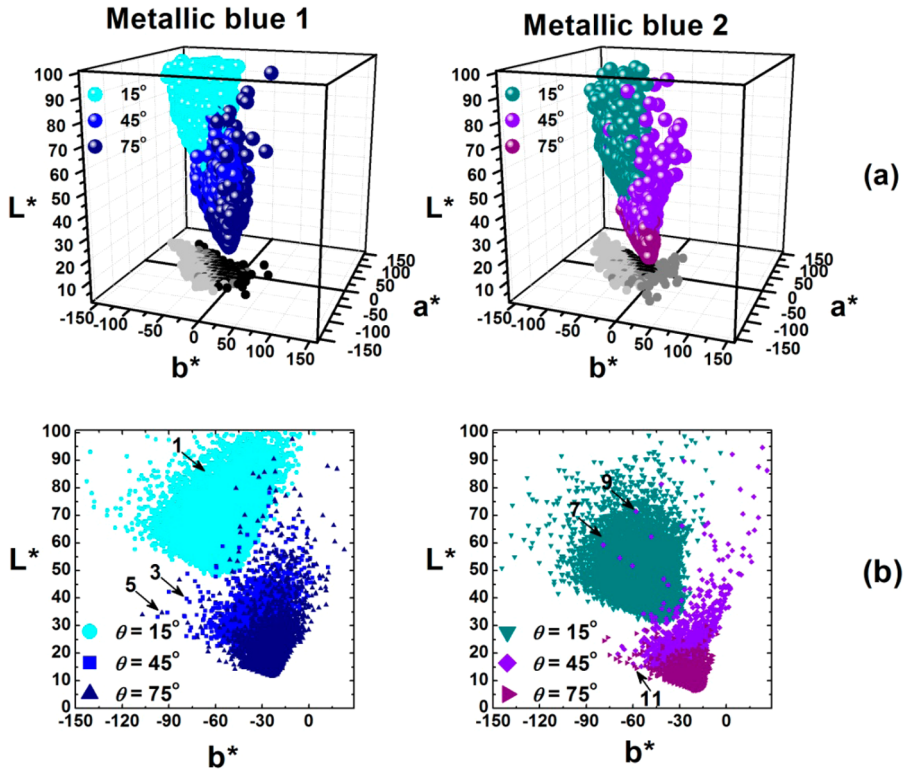

Figure 5. (a) Color coordinates of the entire imaged areas (201 × 201 pixels) in the CIELAB color space. For each CCD pixel, color coordinates were calculated using the CIE 2° standard observer and the D65 illuminant. Each pixel is represented by a single sphere. Each illumination angle is represented by a set of spheres with different colors. Light gray, gray, and dark gray dots indicate the projection in the (a^*,b^*) plane at illumination angles, θ, of 15, 45, and 75°, respectively. (b) Two-dimensional projection in the (L^*,b^*) plane at different illumination angles. Circles, squares, and upward-pointing triangles indicate the color coordinates of metallic blue 1 at 15, 45, and 75°, respectively. Downward-pointing triangles, diamonds, and right-pointing triangles indicate the color coordinates of metallic blue 2 at 15, 45, and 75°, respectively. The size of the symbols was increased to enhance visualization. Arrows with numbers labeled 1−11 indicate selected pixels that contain sparkles shown in Figure 4.

Figure 5a represents the color coordinates of the ROIs in the CIELAB color space at different illumination angles. Each color data set was derived from 40 401 reflectances.

Both metallic coatings span characteristic 3D color maps at different illumination angles and represent the entire color gamut expanded by each metallic coating on the micron scale. The total number of pixels with lightness values $L^* > 100$ was negligible (<250 pixels), and they were not represented.[6,18] Color maps are strongly inhomogeneous, especially at 15 and 45°, where the density of sparkles is higher (Figure 4). Figure 5b shows the 2D projection in the CIELAB (L^*,b^*) plane. The (L^*b^*) plane captures the complete lightness dynamics of sparkles from aluminum flakes relative to their surround. The CCD pixels of sparkles selected in Figure 4 are clearly outside of the main conglomerate of color coordinates created by the surrounding medium, showing higher blue, b^*, and lightness, L^*, values.

Box-Counting Analysis. Noise reduction from the multispectral system was performed by PCA.[32,33] The covariance matrix of reflectances was created, and a basis of 31 orthogonal eigenvectors ($\mathbf{S}_k$) and their corresponding eigenvalues were extracted and ranked. In metallic blue 1, original reflectance spectra at 15, 45, and 75° were projected in a low-dimensional space using the linear combination of the mean reflectance plus the first two ($\mathbf{S}_1 + \mathbf{S}_2$), the first nine ($\mathbf{S}_1 + ... + \mathbf{S}_9$), and the first five eigenvectors ($\mathbf{S}_1 + ... + \mathbf{S}_5$), respectively (see the Supporting Information). In metallic blue 2, original reflectance spectra at 15, 45, and 75° were projected using the mean reflectance plus the first eight ($\mathbf{S}_1 + ... + \mathbf{S}_8$), the first six ($\mathbf{S}_1 + ... + \mathbf{S}_6$), and the first five eigenvectors ($\mathbf{S}_1 + ... + \mathbf{S}_5$), respectively. In each case, the remaining eigenvectors correspond to spatial noise from equipment artifacts and temporal noise (see the Supporting Information).

Figure 6a shows the color coordinates derived from the projected reflectance spectra in the CIELAB (L^*,b^*) plane. In both metallic coatings, the new CIELAB color coordinates preserve the full colorimetric organization derived from the original reflectance spectra (Figure 5b). Figure 6b represents those color coordinates in the (L^*,b^*) plane attributed to spatial noise from the multispectral system.[32,33] The results in Figure 6b clearly show that the color coordinates from spatial noise are clustered in elongate ellipses that resemble diagonal lines. These color maps are closer to the Euclidean dimension of a smooth curve in 1D and do not capture the irregular distribution of color coordinates in Figure 5b. They are the result of very weak spatial patterns associated with noise from the multispectral system filtered by PCA (see the Supporting Information).

Table 1 shows the average box-counting dimension, D_B, of the color coordinates in the CIELAB (L^*,b^*) plane using the CIE standard illuminant D65 at illumination angles, θ, of 15, 45, and 75°, separately. Three different cases were analyzed: those color coordinates obtained from the original reflectance spectra (labeled as original) (Figure 5b), those derived from the reflectance spectra projected over the first few dominant eigenvectors by PCA (labeled as projected) (Figure 6a), and those

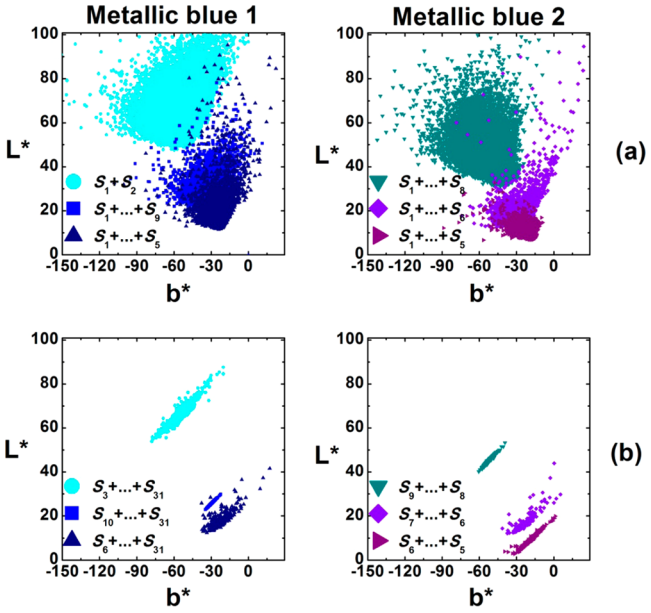

Figure 6. Color coordinates of reflectance spectra generated by PCA in the CIELAB (L^*,b^*) plane at different illumination angles. (a) Color coordinates of reflectance spectra derived from the first dominant eigenvectors $\mathbf{S}_k$, $k\in[1, ..., 9]$. (b) Color coordinates of reflectance spectra derived from those eigenvectors associated with spatial noise from the multispectral system $\mathbf{S}_k$, $k\in[3, ..., 31]$. In all cases, circles, squares, and upward-pointing triangles indicates the color coordinates of metallic blue 1 at illumination angles, θ, of 15, 45, and 75°, respectively. Downward-pointing triangles, diamonds, and right-pointing triangles indicate the color coordinates of metallic blue 2 at 15, 45, and 75°, respectively. The size of symbols was increased to enhance visualization.

color coordinates associated with the spatial noise of the multispectral system (labeled as spatial noise) (Figure 6b).

Linear regression analysis of the total number of grids, $N(r)$, as a function of their size, r, can be fitted by straight lines (in all cases, $R^2 > 0.99$). In both metallic coatings, the box-counting dimension, D_B, is always a noninteger number less than 2, i.e., the Euclidean dimension of the embedded (L^*,b^*) plane. This suggests that the color maps scales in the (L^*,b^*) plane according to a fractal surface of dimension D_B.[19,24,25] There is a significant change in D_B when measured at the illumination angle $\theta = 15°$. This also suggests that the spatial distribution of nearby color coordinates in the (L^*,b^*) plane at $\theta = 15°$ are more irregular or rugged and share a distinct power law when the box size is reduced due to the presence of more sparkles from aluminum flakes. Models of metallic coatings also predict a higher density of sparkles at viewing angles close to the specular reflection, although these models have not described their spectral properties.[36,37]

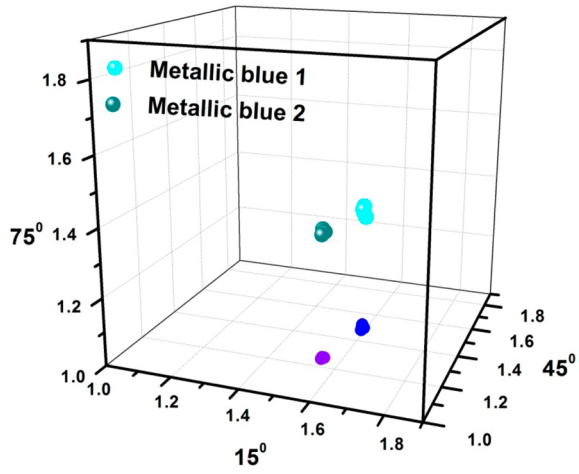

Figure 7. Box-counting dimension, D_B, calculated from the color coordinates of metallic coatings in the CIELAB (L^*,b^*) plane at different illumination angles using the D65, A, FL2, and FL11 illuminant spectra. Each sphere indicates the dimension, D_B, using a different illuminant. Solid circles indicate the projection in the plane that corresponds to illumination angles θ = 15 and 45°.

The D_B values obtained from the original reflectance spectra are similar to those obtained by the projection over the first dominant eigenvectors by PCA; thus, noise artifacts from the multispectral system do not change the main conclusions from box-counting analysis. However, the D_B values derived from the spatial noise of the multispectral system do not capture sparkle effects. They are always lower than the expected value from the original reflectance spectra and fall very close to unity. Noise reduction based on PCA is a robust method that could be used with different effect pigments and concentrations. Comparisons between both metallic coatings reveal that the box-counting dimension, D_B, of metallic blue 2 is slightly smaller at $\theta = 15°$ and clearly different at $\theta = 45°$. This suggests that color maps derived from reflectance spectra in metallic blue 1 are rougher due to the color coordinates generated by sparkles (Figures 4 and 5). Similar conclusions were obtained in terms of the box-counting dimension when the color maps were rescaled to a different value. Finally, Figure 7 represents in a 3D space, the box-counting dimension obtained from the color coordinates projected over the first dominant eigenvectors using the D65, A, FL2, and FL11 illuminant spectra.

The results in Figure 7 clearly show that the box-counting dimension, D_B, differs between metallic blue 1 and metallic blue 2 and is basically independent of the illuminant spectra selected. It is concluded that box-counting analysis of Figures 5b and 6 describes the self-similar properties or how ragged or smooth the color coordinates are clustered on many size scales

Table 1. Box-Counting Dimension, D_B,[a] Derived from the Color Coordinates in the CIELAB (L^*,b^*) Plane Using the CIE Illuminant D65 at Illumination Angles, θ, of 15, 45, and 75°

		θ = 15°	θ = 45°	θ = 75°
metallic blue 1	original	1.623 (±0.006)	1.474 (±0.005)	1.332 (±0.006)
	projected	1.593 (±0.008)	1.493 (±0.006)	1.350 (±0.006)
	spatial noise	1.295 (±0.007)	1.004 (±0.005)	1.189 (±0.007)
metallic blue 2	original	1.558 (±0.006)	1.265 (±0.007)	1.359 (±0.006)
	projected	1.549 (±0.006)	1.259 (±0.007)	1.373 (±0.006)
	spatial noise	1.257 (±0.007)	1.076 (±0.008)	1.193 (±0.008)

[a]Errors in parentheses indicate ±1 standard error of the mean.

in the CIELAB (L^*,b^*) plane. Box-counting provides a robust method for the colorimetric characterization of sparkles relative to their surround. The 3D box-counting space proposed in Figure 7 represents a simple method of classification of micro-brightness in metallic coatings.

CONCLUSIONS

Multispectral imaging is a nondestructive technique that combines both spectral and high-resolution spatial data of surface coatings. It provides more spectral and spatial information than that of the naked eye, RGB-camera based systems, and traditional spectroscopy methods in the characterization of sparkles on the micron scale. Spatial reflectance mapping of typical automotive metallic coatings containing aluminum flakes were performed at different illumination positions from near to far from the surface normal. User-defined ROIs were selected, and reflectance spectra at different CCD pixels were transformed to color coordinates. The spectral signature of pigments at different spatial positions was mapped in a perceptual color space. We conclude that sparkles are outliers in the CIELAB color space. They have color coordinates that present higher lightness values and are far apart from the bulk of color coordinates developed by the surround. Box-counting analysis of color maps has revealed characteristic power laws. Thus, cluster formation of color coordinates is fractal, and the box-counting dimension, D_B, depends on sparkles at different illumination angles and is independent of the illumination spectra. The box-counting dimension, D_B, was higher when sparkles from aluminum flakes dominate at an illumination angle, θ, of 15°, suggesting the existence of rugged color maps. We suggest that the box-counting dimension, D_B, in the color space can be used as a design principle for further enhancement of texture effects in metallic coatings. Although we have focused on automotive OEM metallic coatings, our methods can be extended to any type of surface coatings containing different effect pigments such as mica-based and borosilicate pigments in cosmetics, security inks, and others. Multispectral imaging together with box-counting are valuable tools in texture engineering and could have potential applications for failure analysis and unsupervised detection and classification of sparkles in industrial quality control.

ASSOCIATED CONTENT

Supporting Information

Description of the two-point correlation method; spectral calibration of the multispectral system; and principal component analysis. This material is available free of charge via the Internet at http://pubs.acs.org.

AUTHOR INFORMATION

Corresponding Author

*E-mail: jmedinaru@cofis.es.

Present Address

[†](C.V.) BASF Coatings GmbH, ECO/TBC - 67004, 97080, Wuerzburg, Germany.

Author Contributions

J.M.M. and J.A.D. designed, prepared, and calibrated the multispectral system. J.M.M., J.A.D., and C.V. designed the experiments. J.M.M. performed and analyzed the experiments and drafted the manuscript. J.M.M., J.A.D., and C.V. discussed and revised the manuscript. All authors have read and given approval to the final version of the manuscript.

Notes

The authors declare no competing financial interest.

ACKNOWLEDGMENTS

This research was developed during a visiting research stay of Dr. José M. Medina in the Departmento de Óptica, Universidad de Granada, Spain, supported by the Departmento de Óptica, Universidad de Granada. The authors acknowledge Professor Kenneth Norwich (University of Toronto, Canada) for helping to clarify the text and for discussing the issues and the Color Imaging Group (University of Granada, Spain) for their hardware partial support. J.M.M. and J.A.D. acknowledge the European Regional Development Fund, ERDF, through Programa Operacional Factores de Competitividade, COMPETE (FCOMP-01-0124-FEDER-014588), and National Portuguese funds through the Fundação para a Ciência e Tecnologia, FCT (PTDC/CTM-MET/113352/2009).

ABBREVIATIONS

3D, three dimensional
2D, two dimensional
1D, one dimensional
RGB, red, green, and blue
sRGB, standard red, green and blue color space
OEM, original equipment manufacturer
SEM, scanning electron microscopy
CCD, charge-couple device
LCTF, liquid crystal tunable filter
Hg−Xe, mercury−xenon
CIE, Commission Internationale de l'Éclairage
CIELAB, CIE 1976 $L^*a^*b^*$ perceptual color space
PCA, principal component analysis
ROI, region of interest

REFERENCES

(1) McCamy, C. S. Observation and Measurement of the Appearance of Metallic Materials. Part II. Micro Appearance. *Color Res. Appl.* **1998**, *23*, 362−373.
(2) Maile, F. J.; Pfaff, G.; Reynders, P. Effect Pigments—Past, Present and Future. *Prog. Org. Coat.* **2005**, *54*, 150−163.
(3) Kirchner, E.; Njo, L.; de Haas, K.; Rösler, M. Coarseness and Glints. *Eur. Coat. J.* **2006**, *11*, 46−50.
(4) Kirchner, E.; van den Kieboom, G.-J.; Njo, L.; Supèr, R.; Gottenbos, R. Observation of Visual Texture of Metallic and Pearlescent Materials. *Color Res. Appl.* **2007**, *32*, 256−266.
(5) Cann, A. All about Sparkles. *Opt. Photonics News* **2013**, *24*, 42−45.
(6) Klein, G. A. *Industrial Color Physics*; Springer: New York, 2010.
(7) *Pigment Handbook: Properties and Economics*, 2nd ed.; Lewis, P. A., Ed.; John Wiley & Sons: New York, 1988.
(8) Streitberger, H.-J.; Dössel, K.-F. *Automotive Paints and Coatings*, 2nd ed.; Wiley-VCH: Weinheim, Germany, 2008.
(9) Dekker, N.; Kirchner, E. J. J.; Super, R.; van den Kieboom, G. J.; Gottenbos, R. Total Appearance Differences for Metallic and Pearlescent Materials: Contributions from Color and Texture. *Color Res. Appl.* **2011**, *36*, 4−14.
(10) Huang, Z.; Xu, H.; Luo, M. R.; Cui, G.; Feng, H. Assessing Total Differences for Effective Samples Having Variations in Color, Coarseness, and Glint. *Chin. Opt. Lett.* **2010**, *8*, 717−720.
(11) Huang, Z.; Xu, H.; Luo, M. R. Camera-Based Model To Predict the Total Difference Between Effect Coatings under Directional Illumination. *Chin. Opt. Lett.* **2011**, *9*, 093301.
(12) Amookht, S.; Kandi, S. G.; Mahdavian, M.; Moradian, S. The Effect of Clear Coat and Basecoat Interdiffusion on the Appearance of Automotive Coating System. *Prog. Org. Coat.* **2013**, *76*, 1325−1328.

(13) McCamy, C. S. Observation and Measurement of the Appearance of Metallic Materials. Part I. Macro Appearance. *Color Res. Appl.* **1996**, *21*, 292−304.
(14) Medina, J. M.; Díaz, J. A. Scattering Characterization of Nanopigments in Metallic Coatings Using Hyperspectral Optical Imaging. *Appl. Opt.* **2011**, *50*, G47−G55.
(15) Gat, N. Imaging Spectroscopy Using Tunable Filters: A Review. *Proc. Soc. Photo-Opt. Instrum. Eng.* **2000**, *4056*, 50−64.
(16) *Techniques and Applications of Hyperspectral Image Analysis*; Grahn, H. F.; Geladi, P., Eds.; John Wiley & Sons: Chichester, England, 2007.
(17) Kim, D. B.; Seo, M. K.; Kim, K. Y.; Lee, K. H. Acquisition and Representation of Pearlescent Paints Using an Image-Based Goniospectrophotometer. *Opt. Eng.* **2010**, *49*, 043604.
(18) Wyszecki, G.; Stiles, W. S. *Color Science: Concepts and Methods, Quantitative Data and Formulae*, 2nd ed.; John Wiley & Sons: New York, 1982.
(19) Mureika, J. R. Fractal Dimensions in Perceptual Color Space: A Comparison Study Using Jackson Pollock's Art. *Chaos* **2005**, *15*, 043702.
(20) Chapeau-Blondeau, F.; Chauveau, J.; Rousseau, D.; Richard, P. Fractal Structure in the Color Distribution of Natural Images. *Chaos, Solitons Fractals* **2009**, *42*, 472−482.
(21) Chauveau, J.; Rousseau, D.; Chapeau-Blondeau, F. Fractal Capacity Dimension of Three-Dimensional Histogram from Color Images. *Multidimens. Syst. Signal Process.* **2010**, *21*, 197−211.
(22) Taylor, R. P.; Micolich, A. P.; Jonas, D. Fractal Analysis of Pollock's Drip Paintings. *Nature* **1999**, *399*, 422−422.
(23) Taylor, R. P.; Guzman, R.; Martin, T. P.; Hall, G. D. R.; Micolich, A. P.; Jonas, D.; Scannell, B. C.; Fairbanks, M. S.; Marlow, C. A. Authenticating Pollock Paintings Using Fractal Geometry. *Pattern Recognit. Lett.* **2007**, *28*, 695−702.
(24) Mandelbrot, B. B. *The Fractal Geometry of Nature*; W.H. Freeman Company: San Francisco, CA, 1982.
(25) Mandelbrot, B. How Long Is the Coast of Britain? Statistical Self-similarity and Fractional Dimension. *Science* **1967**, *156*, 636−638.
(26) Kirchner, E. Film Shrinkage and Flake Orientation. *Prog. Org. Coat.* **2009**, *65*, 333−336.
(27) Weldon, D. G. *Failure Analysis of Paints and Coatings*; John Wiley & Sons: Chichester, England, 2009.
(28) Medina, J. M.; Díaz, J. A.; Valero, E.; Nieves, J. L.; Vukusic, P. Detailed Experimental Characterization of Reflectance Spectra of *Sasakia charonda* Butterfly Using Multispectral Optical Imaging. *Opt. Eng.* **2014**, *53*, 033111.
(29) Labsphere Spectralon Diffuse Reflectance Standards. http://www.labsphere.com/products/reflectance-standards-and-targets/spectralon-reflectance-standards.
(30) McCamy, C. S.; Marcus, H.; Davidson, J. G. A Color-Rendition Chart. *J. Appl. Photogr. Eng.* **1976**, *2*, 95−99.
(31) Jolliffe, I. T. *Principal Component Analysis*. 2nd ed.; Springer-Verlag: New York, 2002.
(32) Lopez-Alonso, J. M.; Alda, J.; Bernabeu, E. Principal-Component Characterization of Noise for Infrared Images. *Appl. Opt.* **2002**, *41*, 320−331.
(33) Lopez-Alonso, J. M.; Alda, J. Characterization of Hyperspectral Imagers and Scenes: Background and Equipment Artifacts. *Proc. Soc. Photo-Opt. Instrum. Eng.* **2004**, *5612*, 265.
(34) Karperien, A. FracLac for ImageJ. http://rsb.info.nih.gov/ij/plugins/fraclac/FLHelp/Introduction.htm (accessed 1993).
(35) Schneider, C. A.; Rasband, W. S.; Eliceiri, K. W. NIH Image to ImageJ: 25 Years of Image Analysis. *Nat. Methods* **2012**, *9*, 671−675.
(36) Ershov, S.; Khodulev, A.; Kolchin, K. *Simulation of Sparkles in Metallic Paints*, Proceedings of the International Conference on Computer Graphics and Vision (GraphiCon), Moscow, Russia, August 26−September 1; GraphiCon: Moscow, Russia, 1999.
(37) Ferrero, A.; Campos, J.; Rabal, A. M.; Pons, A. A Single Analytical Model for Sparkle and Graininess Patterns in Texture of Effect Coatings. *Opt. Express* **2013**, *21*, 26812−26819.